

Computational Investigation of Flow and Heat Transfer in a Rectangular Duct with Ribs Mounted in a Staggered Arrangement

M. Alhajeri*

Mechanical P& R Engineering Department, Faculty of Technological Studies, PAAET, Kuwait

Abstract

Fluid Flow and heat transfer results are presented from a ribbed U-tube, which models passages used to cool the blades in gas turbine engines. Computational fluid dynamics is used here to predict the air flow behavior and the surface Nusselt number distributions. The model of the coolant passage consists of two square legs that are connected by a sharp, 180-degree bend with a rectangular outer wall. Four ribs are placed in each side of the leg and mounted in a staggered arrangement. The height and width of the rib are equal to 0.1 duct width, and the rib spacing is 10 times the rib height. Based on inlet flow conditions, the Reynolds number (Re) is 95000. It was found that, after the flow resettles from the disturbances created by the obstacle of the first rib or the effect of the bend, the flow forms two re-circulations, a large one behind the rib and a small one ahead of the rib. The maximum values of the Nusselt numbers are located at a distance of almost one rib height h ahead of the flow reattachment point.

Keywords: *Turbine blade cooling, CFD, Rib.*

1. Introduction

In aircraft gas turbine engines, both high thermal efficiency and specific thrust are dependent upon turbine inlet gas temperature, which is limited by the thermal properties of the turbine blade materials and their internal cooling capabilities. Sufficient cooling of the turbine blades allows their environmental operating temperature to exceed the material's melting point without affecting the integrity of the blades. A number of investigations have been conducted using various rectangular channels with 180° turns. Metzger and Sham [1] studied heat transfer effects around smooth rectangular channels with sharp, 180° turns. Carlomagno [2] reported heat transfer measurements performed by means of infrared thermography in an internal flow through a 180° turn in a square channel, which is relevant to the internal cooling of gas turbine blades. He showed that the Nusselt number increased ahead of the bend, while some very high heat transfer coefficient regions were present at the wall towards the partition wall axis. Arts et al. [3] investigated the flow and heat transfer in a straight-ribbed cooling channel. They found that the pressure coefficient C_p increases before the ribs and decreases after the ribs. No significant difference in turbulence intensity was found when the rib spacing was varied. Regions of high heat transfer were found in the vicinity of the reattachment location and before the ribs. Cakan and Arts [4] also studied the flow in a similar test section using Particle

Image Velocimetry (PIV). They found that the flow through the ribbed channel could be characterized by a series of accelerations, decelerations with separation, reattachment and redevelopment due to the sudden changes in cross-sectional area. The ribs induce a separation and recirculation bubbles. Comparing both studies, no Reynolds number dependency of reattachment distance was found. The flow in a straight, rectangular channel with ribs on the two opposite walls was investigated by Liou et al. [5, 6], and the flow in a rectangular channel with a 180-degree bend was investigated by Schabacker et al. [7] and Servouze et al. [8]. Iacovides et al. [9] conducted a Laser Doppler Anemometry (LDA) investigation of the flow at a Reynolds number of 100,000 in a ribbed channel with a 180-degree turn. The ratio of the height of the rib to the diameter of the duct was 0.1. They observed a periodic flow behavior. Due to existence of the ribs, turbulence increases at the entrance to the bend, and an additional separation bubble is formed over the first rib interval downstream of the bend exit. Amro et al. [10] conducted an experimental study of heat transfer in a ribbed cooling channel. They found that the most promising rib arrangement for leading edge cooling is a rib with a 45-degree angle and double-sided, fully-overlapped ribs in the arc area. These ribs provide uniform heat transfer in the arc area and result in high values for the heat transfer coefficients in the channel. Jia et al. [11] reported on a numerical analysis of heat transfer enhancement in square ducts with V-shaped ribs. They found that, both downstream and upstream of the bend, V-shaped ribs result in better heat transfer enhancement than transverse straight ribs in ducts. Sewall and Tafti [12] carried out a large

* Corresponding author.

E-mail: eaxalm@yahoo.com

© 2011 International Association for Sharing Knowledge and Sustainability

DOI: 10.5383/ijtee.04.01.012

eddy simulation of a 180-degree bend or bend in a stationary ribbed duct. The domain studied includes three ribs upstream of the bend region and three ribs downstream of the bend with an outflow extension added to the end. They found that heat transfer is increased with the presence of a rib. Including a rib in the bend increases the friction factor in the bend by 80%, and it increases the heat transfer augmentation by approximately 20%, resulting in a trade-off between pressure drop and heat transfer. Numerical predictions of a hydrodynamic and thermally-developed turbulent flow are presented by Aroon et al. [13] for a rotating duct with square ribs aligned normally to the main flow direction. Another computational simulation was performed by Tafti [14] in a ribbed square duct with a rib height to hydraulic diameter ratio of 0.1 and a rib pitch to rib height ratio of 10. Computational investigation of a rib-roughened U-bend at high Reynolds number (Re = 95000) is done by Bredberg and Davidson [15]. They found that the heat transfer is increased downstream from the bend due to the higher turbulence level. The aim of this study is to investigate numerically the velocity field, turbulence intensity, and heat transfer in a U-bend tube (sharp 180-degree turn) with square ribs. The work in this study will be compared with similar work from the pertinent literature.

2. Mathematical Modeling

The equations governing the steady flow of a two-dimensional, incompressible fluid are the differential expressions for mass, momentum, and energy conservation. These are given by:

$$\frac{\partial u}{\partial x} + \frac{\partial v}{\partial y} = 0 \quad (1)$$

$$g_x - \frac{1}{\rho} \frac{\partial p}{\partial x} + v \left(\frac{\partial^2 u}{\partial x^2} + \frac{\partial^2 u}{\partial y^2} \right) = u \frac{\partial u}{\partial x} + v \frac{\partial u}{\partial y} \quad (2)$$

$$g_y - \frac{1}{\rho} \frac{\partial p}{\partial y} + v \left(\frac{\partial^2 v}{\partial x^2} + \frac{\partial^2 v}{\partial y^2} \right) = u \frac{\partial v}{\partial x} + v \frac{\partial v}{\partial y} \quad (3)$$

Where $\nu = \frac{\mu}{\rho}$

$$\rho C_p \left(U \frac{\partial T}{\partial X} + V \frac{\partial T}{\partial Y} \right) = \frac{\partial}{\partial X} \left(k \frac{\partial T}{\partial X} \right) + \frac{\partial}{\partial Y} \left(k \frac{\partial T}{\partial Y} \right) \quad (4)$$

The standard k-ε model is a semi-empirical model based on model transport of equations for the turbulent kinetic energy (k) and its dissipation rate (ε) (Tutar and G. Oguz [16]). The turbulent kinetic energy, k, and its rate of dissipation, ε, are obtained from the following transport equations:

$$\rho \frac{Dk}{Dt} = \frac{\partial}{\partial x_j} \left[\left(\mu + \frac{\mu_t}{\sigma_k} \right) \frac{\partial k}{\partial x_i} \right] + G_k + G_b - \rho \varepsilon - Y_M \quad (5)$$

$$\rho \frac{D\varepsilon}{Dt} = \frac{\partial}{\partial x_j} \left[\left(\mu + \frac{\mu_t}{\sigma_k} \right) \frac{\partial \varepsilon}{\partial x_i} \right] + C_{1\varepsilon} \frac{\varepsilon}{k} (G_k + G_{3\varepsilon} G_b) - C_{2\varepsilon} \rho \frac{\varepsilon^2}{k} \quad (6)$$

In these equations, G_k represents the generation of turbulent kinetic energy due to mean velocity gradients, G_b is the generation of turbulent kinetic energy due to buoyancy, and Y_M represents the contribution of the fluctuating dilatation in compressible turbulence to the overall dissipation rate.

The term G_k , which represents the production of turbulent kinetic energy, is defined as:

$$G_k = -\rho u_i' u_j' \frac{\partial u_j}{\partial x_i} \quad (7)$$

To evaluate G_k in a manner with the Boussinesq hypothesis (Tutar and G. Oguz [16]),

$G_k = \mu_t S^2$, where S is the modulus of the mean rate-of-strain tensor, defined as:

$S = \sqrt{2S_{ij}S_{ij}}$ with mean S_{ij} given by

$$S_{ij} = \frac{1}{2} \left(\frac{\partial u_i}{\partial x_j} + \frac{\partial u_j}{\partial x_i} \right) \quad (8)$$

Now, G_b is the generation of turbulent kinetic energy due to buoyancy.

$$G_b = \beta g_i \frac{\mu_t}{Pr_t} \frac{\partial u_j}{\partial x_i} \quad (9)$$

Where Pr_t is the turbulent Prandtl number for energy. For standard k-ε models, the default value of Pr_t is 0.85

β is the coefficient of thermal expansion and is defined by:

$$\beta = -\frac{1}{\rho} \left(\frac{\partial \rho}{\partial T} \right)_p \quad (10)$$

The “eddy” or turbulent viscosity, μ_t , is computed by combining k and ε as follows:

$$\mu_t = \rho C_\mu \frac{k^2}{\varepsilon} \quad (11)$$

The model constants $C_{1\varepsilon}, C_{2\varepsilon}, \sigma_k$ and σ_ε have the following default values

$$C_{1\varepsilon}=1.44, C_{2\varepsilon}=1.92, \sigma_k=1.0, \sigma_\varepsilon=1.3, C_\mu=0.09, C_{3\varepsilon}=1$$

Default values have been determined from experiments with air and water for fundamental turbulent shear flows, including homogeneous shear flows and decaying isotropic grid turbulences. These values have been found to work fairly well for a wide range of wall-bounded and free-shear flows.

3. Geometry and Boundary Conditions

Sixteen square ribs are simulated in a tube with a sharp bend. Four ribs are placed in each side of the tube upstream from the bend, and the same number and arrangement of ribs are placed in the tube downstream from the bend, as shown in Fig. 1. The U-tube has a width of d with a 180° bend with a mean radius,

rc/d , equal to 0.65. The ribs are distributed on both walls in a staggered arrangement. The ratio of the height of the rib to the diameter of the tube, h/d , is 0.1, and the ratio of the spacing between the ribs to the diameter of the duct, S/d , is one. The ribs closest to the bend are at 0.45d from the entrance and exit of the bend. Finally, the ratio of the height of the rib to the width of the rib, h/w , is one.

The mesh or grid is a structured-type cell (Quad cell) and is generated in Gambit. The cells are concentrated near the upper and bottom walls with distance h from the wall. However, in the middle, the mesh is uniform between the head of the ribs with a distance of $d-2h$ in the y direction. The total grid size is 64260 quadrilateral cells. The domain is a two-dimensional plane and has three boundaries, as shown in Fig. 1. The inflow boundary or the main inlet is set as a constant x -component and zero y -component of the velocity. The inlet velocity in the x -direction is found to be 10 m/s. At the outflow boundary, the velocities are left free so that the default boundary condition of zero stress in normal and tangential directions is obtained. The boundary conditions at the wall set as wall cell using the standard wall function. A no-slip velocity boundary condition is applied at the wall, i.e., both the x - and y -components of velocity are constrained to be zero. Furthermore, the CFD code used here is Fluent and Gambit for meshing.

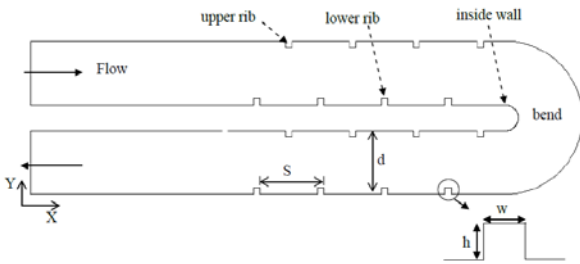


Figure 1. The geometry of the square rib case

4. Validation and Grid Independency

Three square rib cases were modeled (coarse, fine, and dense) to check the grid's independency, and it was enough to reach the grid independency. The fine case, with an interval count of 0.07 (as described in Gambit) and 110334 cells, is chosen. Numerical simulation of a rib-roughed U-tube at high Reynolds number (95000) is presented by Bredberg and Davidson [15]. They compared their results with measurement data obtained by Iacovides and Launder [17], and they found excellent agreement between the two results (numerical and measurement). The results obtained by Bredberg and Davidson [15] will be compared and validated with the results achieved in this study, since their results are already validated with experimental work. Fig. 2a shows the work done in this study, while Fig. 2b presents the similar geometry and boundary conditions simulated by Bredberg et al. [15]. The Figures show that the two findings are closely matched.

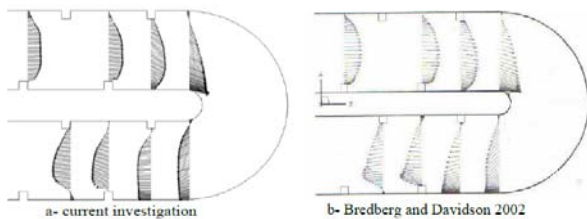


Figure 2. comparison between two velocity vector profiles for square rib

Fig. 3 shows comparisons with experimental results obtained by Iacovides and Launder [9] for a velocity profile at $x = 36$ upstream of the bend for a square rib (x is the distance from the left side of the duct which is the inlet and outlet of the duct). The two profiles are closely matched, especially in the area close to the wall, which is the area of interest in our current study. In the middle of the duct, the profile in the experimental results curve more than in computational results.

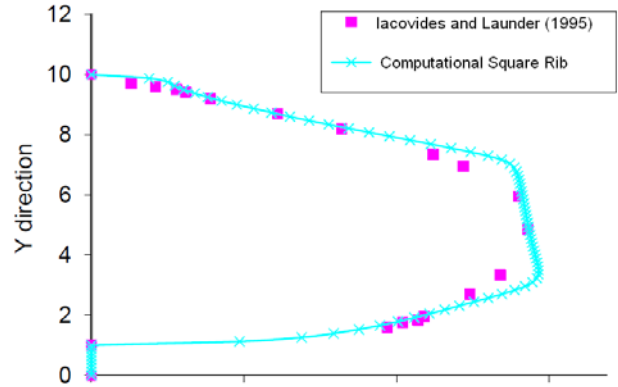


Figure 3. Comparison with experimental results obtained by Iacovides and launder [16] for velocity profile at $x = 36$ upstream of the bend for square rib

5. Results and Discussion

5.1 Flow Field

The velocity profiles in Fig. 4 indicate that there are eddies between the ribs. At the first rib and behind the first rib, no recirculation appeared at the opposite wall. However, flow in the opposite direction from the mean flow could be seen at the top of the rib and behind it. After the second rib, flow in the opposite direction from the main stream is also clear.

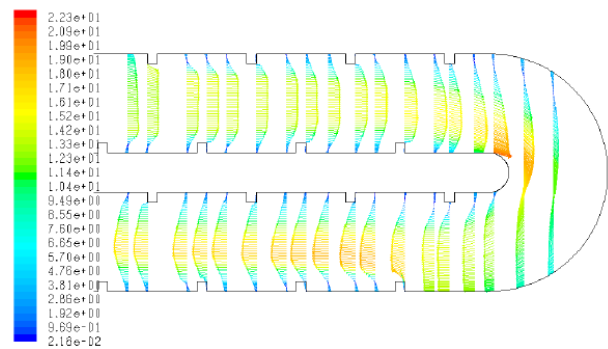


Figure 4. velocity profiles at different x-distances (m/s)

Large eddies occurred near the wall at the top of the bend, because the last rib in the upstream tube is located in the top wall. These eddies reduced the diameter that allow the air to flow and increase the velocity to the maximum inside the bend, satisfying the continuity equation. The flow could not follow the downstream curve of the bend, and the second largest eddy formed near the upper wall of the downstream tube. The size of this eddy allowed it to reach the third rib, generating a high-velocity region in the middle of the tube. At the last five ribs, the reverse flow that creates the eddies no longer existed. Velocity vectors of geometry are shown in Figs. 5 and 6. The geometry is divided into parts so that the recirculation can be clearly seen. The lengths of the vectors are set at a fixed value

to show the low velocity region. Fig. 5a shows the first upstream part, which are the first four ribs. The separation started at a distance equal to the rib height (h) before the rib, and reattachment occurred at a distance about 7h between the first two ribs and 5h between the ribs for the subsequent ribs. At the bottom of the last upstream rib, recirculation is reduced in size due to the movement of the high velocity region toward the lower wall to enter the opening of the downstream tube. Large eddies, which cover half of the bend's outer distance, are created just after the last upper rib.

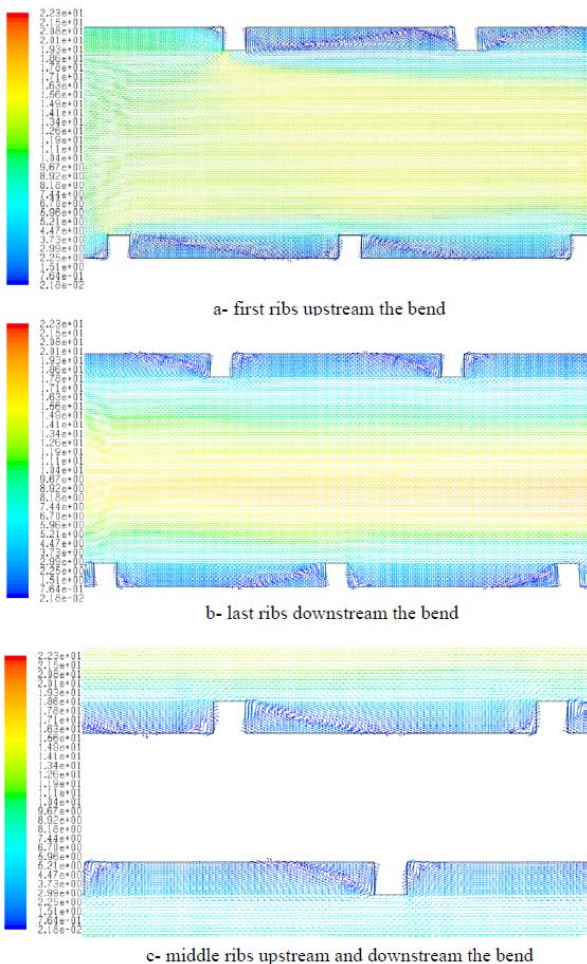


Figure 5. Velocity vectors for different locations (m/s)

Two large recirculations are present before and after the first rib downstream, covering the whole area, including the rib. This is due to centrifugal force in the bend that causes the flow to go far from the upper wall toward the lower wall, forcing the flow to separate before the second downstream rib. The size of the recirculation region behind the rest of the ribs shrank to almost 4h of the rib, allowing the main stream to contact the wall. Furthermore, the ribs quickly dominate the flow and thus lead to a fast recovery of the flow from the bend effect. Stream function contours are shown in Fig. 7. It can be noticed from the contours that the recirculation behind most of the ribs, except for the ribs near the bend and the entrance, was comparatively small.

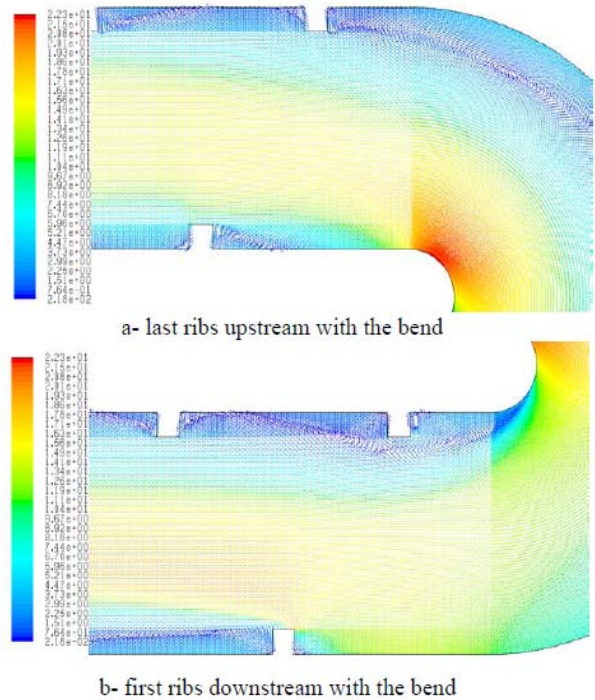


Figure 6. Velocity vectors for different locations

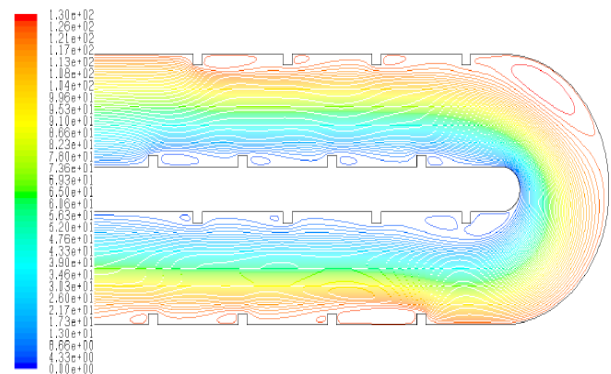


Figure 7. Stream functions contours

The velocity profiles for the three walls with their ribs (downstream upper and lower walls and upstream lower wall) are shown in Figs. 8, 9, and 10. (The gray, vertical, thick lines in these Figures show the locations of the ribs.) Two velocity profiles are considered here at the y-axis (direction) i.e., one at the middle of the ribs and the second at the top of the ribs. Those locations for the middle of the rib are 14.5, 9.5 and 0.5, and, for the top of the ribs, they are 15, 9 and 1 for both profiles, respectively, for lower ribs upstream, upper ribs downstream, and lower ribs downstream of the bend. For all those Figures, the discussion starts with the direction of the flow, as stated in the figures, which means that the first rib in each Figure is the first one in the direction of the flow.

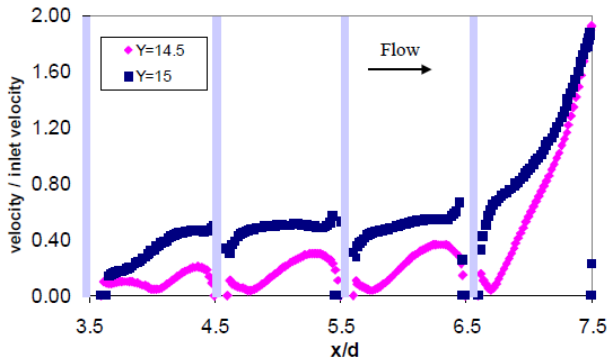


Figure 8. velocity profiles at the middle of the rib (y=14.5) and top of the rib (y=15) for lower ribs upstream of the bend

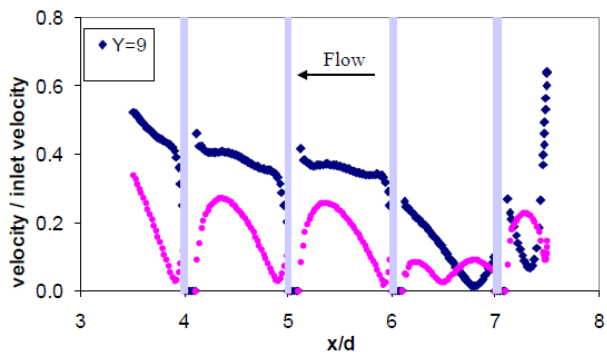


Figure 9. velocity profiles at the middle of the rib (y=9.5) and top of the rib (y=9) for upper ribs downstream of the bend

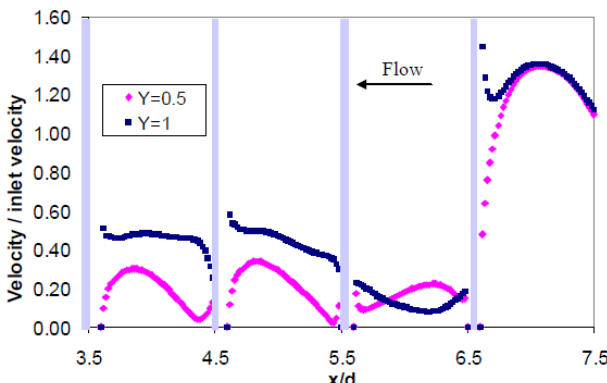


Figure 10. velocity profile at the middle of the rib (y=0.5) and top of the rib (y=1) for lower ribs downstream of the bend

The velocity profiles for the lower ribs upstream of the bend for the two locations in the y-direction (y = 14.5 and y = 15) are shown in Fig. 8. For the profile at the middle of the rib, the recirculation is larger after the first rib, giving the first rib the lowest velocity profile of all the ribs. After the second and third ribs, the behaviors are identical. Here, the recirculation is smaller than after the first rib. This is due to the fact that the air before the first rib flows with higher velocity and momentum close to the wall, and, when it faces an obstacle (rib), it separates before the first rib and takes a long distance to reattach, creating large recirculation. However, after the first rib, the mainstream moves between the heads of the ribs, leaving the area between the ribs with lower velocities and momentum, so the flow is able to reattach faster after each separation, creating higher velocities between the ribs and smaller recirculation. After the fourth (last) rib, the flow, after very small recirculation, encounters the change in the geometry in the bend, where the higher velocity region moves toward the

closest distance, i.e., the inside wall of the bend. This is why the velocity value is increased here by a factor of nine over the velocity after the first rib. For the profile at the top of the head (y = 15), the flow is out of the recirculation region after the second and third ribs, and the velocity here is greater than the velocity after the first rib.

Fig. 9 shows the velocity profiles at the middle of the rib (y = 9.5) and the top of the rib (y = 9) for the upper wall ribs downstream of the bend. We will start this time from the right in the Figure, because this is downstream of the bend, and the flow comes from there (from the bend). For the profile at the top of the rib (y = 9), the flow enters the downstream tube with a high velocity, because, as we discussed earlier, a large recirculation occurs near the outside wall of the bend, reducing the area for flow and creating a high-velocity region. After a very short distance, the velocity decreases rapidly to reach a value lower than that for the second profile (y = 9.5). This is due to the action of centrifugal force when the flow is turning with high velocity and momentum as it enters the downstream tube, creating the largest recirculation in the upper wall. This shifts the center of the recirculation far from the wall, at distance larger than the rib height. Another large recirculation occurs after the first rib because of the turning of the flow far from the upper wall, creating recirculation with its center at a distance equal to the rib height. This generates a low velocity that reaches zero, because the velocity profile is passing the center of the recirculation. The flow behaviors are similar to those shown in Fig. 8 for other ribs.

Velocity profiles at the middle of the rib (y = 0.5) and at the top of the rib (y = 1) for the lower ribs downstream of the bend are shown in Fig. 10. As mentioned in the previous paragraph, it is clear that the centrifugal force shifts the high-velocity region next to the lower wall. The flow enters the tube with very high velocity normal to the wall, increasing the friction and, consequently, increasing the heat transfer. After striking the wall, the flow moves far from the wall, creating a large recirculation and decreasing the velocity after the first rib, especially at the height of the rib.

The turbulence intensity, also often referred to as turbulence level, is defined as:

$$I = \frac{u'}{U} \tag{12}$$

Where u' is the root-mean-square of the turbulent velocity fluctuations and is the U e mean velocity (Reynolds averaged). If the turbulent energy, k , is known, u' can be computed as:

$$u' = \frac{1}{3}(u_x'^2 + u_y'^2 + u_z'^2)^{0.5} = \left[\frac{2}{3}k\right]^{0.5} \tag{13}$$

U can be computed from the three mean velocity components U_x , U_y and U_z as:

$$U = [U_x^2 + U_y^2 + U_z^2]^{0.5} \tag{14}$$

The turbulence intensity is higher downstream from the bend, near and between the ribs, and in the bend, as shown in Fig. 11. This means that the purpose of designing the cooling duct with ribs is achieved by increasing the turbulence level near the wall. Fig. 12 shows that higher pressure drops occur in the bend. In addition, there are significant pressure drops at the first two ribs.

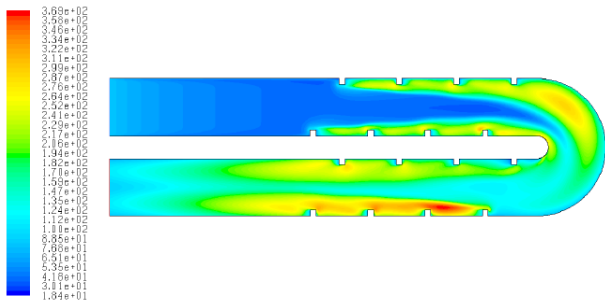


Figure 11. Turbulence intensity

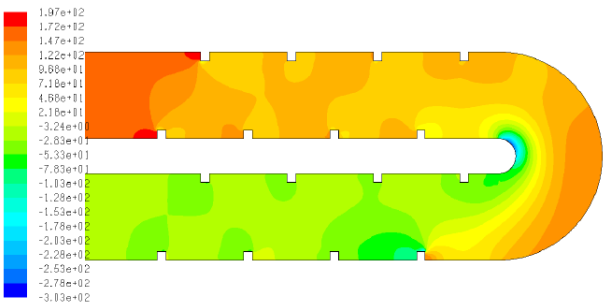


Figure 12. Static pressure (Pascal)

5.2 Heat transfer between the ribs

Internal cooling with ribs is used to enhance the heat transfer inside the blade. The rib increases turbulence in the duct and this increases the heat transfer coefficient. Fig. 13 shows the Nusslet number (Nu) distributions between the lower ribs downstream the bend or at the y-distance equal to zero (y = 0). The Nusslet number is normalized by dividing it by the Nu for a straight tube without ribs, and the distance is divided by the tube diameter. Fig. 13 shows that the Nu is measured starting just after the bend to distance 5h downstream of the last rib. The peaks or maxima are found just after the midpoint between the first two ribs, as counted in direction of flow. The Nu values increase gradually, as opposed to the sharp increments that will be seen later for other ribs. This is because, between those two ribs, there is a large recirculation and the center of the recirculation is approximately a distance of 1h from the wall. Since the center of the recirculation moves in the direction of flow, it moves closer to the wall, increasing the friction and the Nusslet number at the surface of the wall. The phenomena are similar between the second and third ribs and between the third and fourth ribs. In those locations, the maxima are located behind the second and third ribs. This is due to the formation of recirculation just behind each rib, because the flow separates at the edge of the each rib. Then, the Nu decreases after the flow reattaches until it reaches the position of the small recirculation just before the rib where the curve travels horizontally at a constant velocity before it decreases at the rib. It can be noticed here that heat transfer augmentation at the wall surface occurs when the flow creates recirculations with centers near or at the wall.

The Nusslet number distributions between the upper ribs downstream the bend are shown in Fig. 14. In this side of the tube, the Nu does not reach the value that it had in the lower side, except between the last two ribs. The reason is that centrifugal force is acting on the flow in the bend and forcing the flow to move far from the center of the bend. This will result in less friction in the upper side of the tube and, consequently, less heat transfer. The first two ribs are located near the center of the bend, and the flow is moved far from the

wall, creating recirculations with centers that are located far from the surface of the wall, i.e., a distance that is greater than the rib height. This is why the Nu value is small compared to its value at other locations. Dividing the area of the bend by placing thin vanes to prevent the flow from moving far from the inside wall will help to increase the Nusslet number in the upper side of the tube. This must be studied in detail to see whether it justifies the manufacture of small turbine blade with those dividers. As the flow proceeds downstream from the bend, the Nu increases because the flow again fills the entire tube.

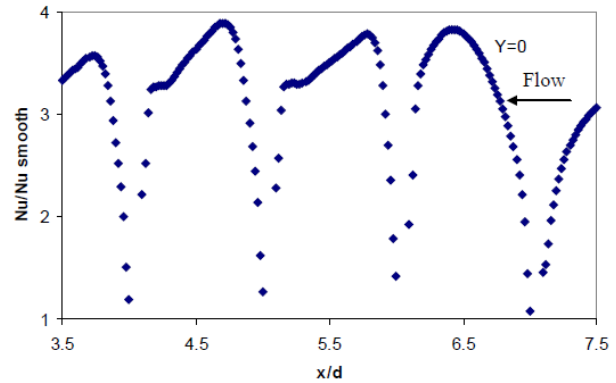


Figure 13. Nusslet number distributions between the lower ribs downstream the bend

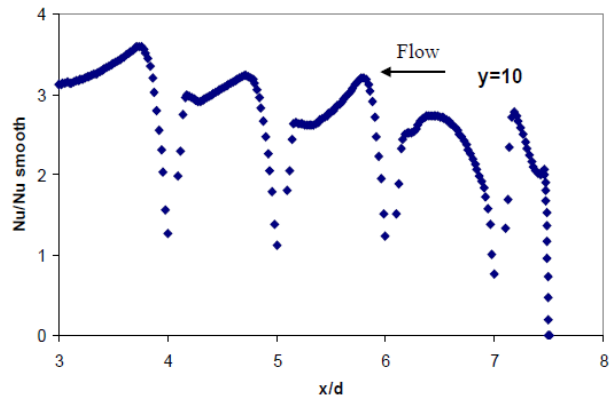


Figure 14. Nusslet number distributions between the upper ribs downstream the bend

The Nusslet number distributions between the lower ribs upstream from the bend are shown in Fig. 15. In this study, the Nusslet number reaches its maximum value behind the last rib on the inside wall in the bend. Recalling Fig. 6, the maximum velocity occurred at the inside wall of the bend, increasing the friction and extracting more heat. The heat transfer behaviors for other ribs are shown to be similar in Figs. 15 and 16, where the maximum Nusslet number always occurs behind each rib due to the existence of recirculation in those positions. The difference between the Nusslet numbers in the smooth tube, where the first almost half of the duct is modeled as smooth tube, and in the ribbed tube is clear in those two Figures. In the case of ribbed tube, the Nu is almost double the value observed in the smooth tube.

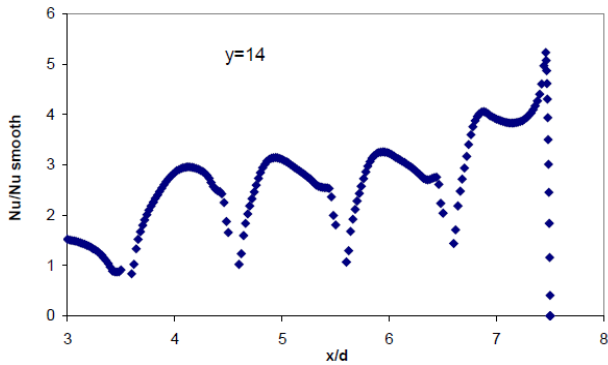


Figure 15. Nusselt number distributions between the lower ribs upstream the bend

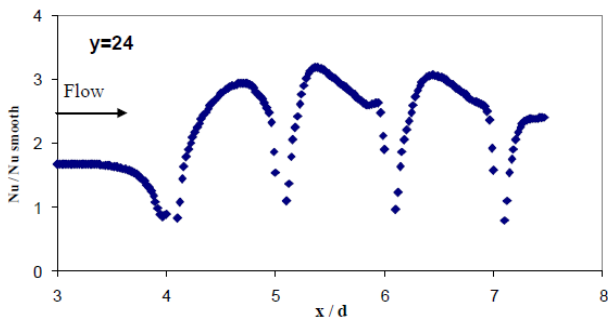


Figure 16. Nusselt number distributions between the upper ribs upstream the bend

In general, for the Nusselt number distribution between the ribs that are located far from the bend and after the first rib, the Figures show two peaks; one is visible behind the rib, and the second, very small peak is visible just before the rib. The larger peak is located at a distance almost one rib height h ahead the reattachment point. Furthermore, it is found that heat transfer is enhanced if there is recirculation and the velocity in the y -direction is increased. Both make the fluid impact with the wall, increasing the friction and causing more heat to be extracted from the wall.

6. Conclusions

An investigation of the flow and heat transfer in a two-pass, internal coolant passage (tube) was presented. Four ribs were installed in each wall of the tube with a total of sixteen. The study focuses on the flow characteristic effects on the wall and heat transfer distribution. It is concluded that the recirculation regions are reduced after the first rib and increased behind the last rib upstream from the bend. Large recirculation in the upper and outer side of the bend occurred. Two recirculations appeared near the upper and lower first ribs downstream from the bend, and, after that, the recirculations reduce in size and maintain the same behaviors in most cases. High velocity regions are found in the inner side of the bend and after the first lower rib downstream from the bend. Further, the ribs quickly dominate the flow and thus lead to a fast recovery of the flow from the bend effect. Pressure drop occurred after each rib, however most of the pressure loss is in the bend and after the first rib. Turbulence intensities are high at the head of the ribs, between the ribs, and in the bend.

After the first rib in each side and after the bend, two peaks are found for the Nusselt number distribution between the ribs, one behind the rib and the other just ahead of it. The larger peak is located at a distance almost one rib height h ahead of the reattachment point. Furthermore, it is found that heat transfer is

improved with recirculation and increase in velocity in the y -direction. Both make the fluid particles affect the wall, increasing the friction and causing more heat to be extracted from the wall. Furthermore, it is found that heat transfer increased at the wall surface when the centers of the recirculation move toward the wall.

Nomenclature

- K kinetic energy of the turbulence
- G generation of turbulent kinetic energy
- S modulus of the mean rate-of-strain tensor
- T Temperature
- u mean velocity
- u' fluctuating velocity
- x distance from the left side of the duct which is the inlet and outlet of the duct)
- β coefficient of thermal expansion
- ε dissipation rate
- μ viscosity
- μ_t turbulent dynamic viscosity
- ρ Density

References

- [1] D. E. Metzger, and M.K. Sham, Heat transfer Around Sharp 180° Turns in Smooth Rectangular Channels, *Journal of Heat Transfer*, 108 (1986) 500-506. [doi:10.1115/1.3246961](https://doi.org/10.1115/1.3246961)
- [2] G. M. Carlomagno, Quantitative infrared thermography in heat and fluid flow *Optical Methods and Data Processing in Heat and Fluid Flow*, in: IMechE Conference Transaction, England, (1996) 279-290.
- [3] T. Arts, G. Rau, M. Cakan, J. Vialonga, D. Fernandez, F. Tarnowski, E. Laroche, Experimental and numerical investigation on flow and heat transfer in large-scale, turbine cooling representative rib-roughened channels *Journal of Power and Energy*, 211 (1997) 263-272.
- [4] N. Cakan, T. Arts. Effect of Main and Secondary Flows on Heat Transfer in a Rib-Roughened Internal Cooling Channel. 4th International Symposium on Experimental & Computational Aerothermodynamics of Internal Flows, Dresden, Germany, (1999).
- [5] T.-M. Liou, Y.-Y. Wu. LDV Measurements of Periodic Fully Developed Main and Secondary Flows in a Channel With Rib-Disturbed Walls. *Journal of Fluids Engineering*, 115 (1993) 109-114. [doi:10.1115/1.2910091](https://doi.org/10.1115/1.2910091)
- [6] T.-M. Liou, C.-W. Kao, S.-H. Chen. Flow field Investigation of the Effect of Rib Open Area Ratio in a Rectangular Duct. *Journal of Fluids Engineering*, 120 (1998) 504-512. [doi:10.1115/1.2820691](https://doi.org/10.1115/1.2820691)
- [7] J. Schabacker, A. B. Aölcs, B.V. Johnson. PIV Investigation of the Flow Characteristics in an Internal Coolant Passage with 45° Rib Arrangement." ASME Paper 99-GT-120 (1999).

- [8] Y. Servouze, P. Gicquel, E. Saccardi, B. Tanguy, V. Sauter. 3D laser anemometry in a rotating cooling ribbed U-channel." XIV Symposium ISOABE, Florence, Italy (1999).
- [9] H. Iacovides, D. C. Jackson, H. Ji, G. Kelemenis, B. E. Launder, K. Nikas. LDA Study of the Flow Development Through an Orthogonally Rotating U-Bend of Strong Curvature and Rib-Roughened Walls.", *Journal of Turbomachinery*, 120 (1998) 386-391.
- [10] M. Amro, B. Weigand, R. Poser, M. Schnieder, An experimental investigation of the heat transfer in a ribbed triangular cooling channel, *International Journal of Thermal Sciences*, 46 (2007) 491–500. [doi:10.1016/j.ijthermalsci.2006.07.004](https://doi.org/10.1016/j.ijthermalsci.2006.07.004)
- [11] R. Jia, B. Sunden and M. Faghri, Computational Analysis of Heat Transfer Enhancement in Square Ducts With V-Shaped Ribs: Turbine Blade Cooling, *Journal of Heat Transfer*, 127 (2005) 425-433. [doi:10.1115/1.1865220](https://doi.org/10.1115/1.1865220)
- [12] E. Sewall, D. Tafti, Large Eddy Simulation of Flow and Heat Transfer in the 180-Deg Bend Region of a Stationary Gas Turbine Blade Ribbed Internal Cooling Duct, *Journal of Turbomachinery*, 128 (2006) 763-771. [doi:10.1115/1.2098769](https://doi.org/10.1115/1.2098769)
- [13] Aroon K. Viswanathan, Danesh K. Tafti, Detached eddy simulation of flow and heat transfer in fully developed rotating internal cooling channel with normal ribs, *International Journal of Heat and Fluid Flow* 27 (2006) 351–370. [doi:10.1016/j.ijheatfluidflow.2005.12.003](https://doi.org/10.1016/j.ijheatfluidflow.2005.12.003)
- [14] D.K. Tafti, Evaluating the role of subgrid stress modeling in a ribbed duct for the internal cooling of turbine blades, *International J. of Heat and Fluid Flow* 26 (2005) 92–104. [doi:10.1016/j.ijheatfluidflow.2004.07.002](https://doi.org/10.1016/j.ijheatfluidflow.2004.07.002)
- [15] J. Bredberg and L. Davidson, Prediction of turbulent heat transfer in stationary and rotating U-ducts with rib roughened wall, 5th International symposium on engineering turbulence modeling and experiments conference (2002).
- [16] M. Tutar and G. Oguz, Computational Modeling of Wind Flow Around a Group of Buildings, *International Journal of Computational Fluid Dynamics*, December 18 (2004) 651–670
- [17] H. Iacovides, B. Launder, Computational fluid dynamics applied to internal gas turbine cooling, *International Journal of heat and Fluid Flow*, 16 (1995) 454-470. [doi:10.1016/0142-727X\(95\)00072-X](https://doi.org/10.1016/0142-727X(95)00072-X)